COMPUTER-AIDED OPTIMAL DESIGN AND ANALYSIS OF SYMMETRIC SINGLE-AXIS FLEXURE HINGES

SHENYUAN DAI[1], CHONGXIANG LI[1], YUE YU[1], LIFANG QIU[1,*]

Abstract. This paper studies the performance of symmetric single-axis flexure hinges, including their capacity of rotation, precision of rotation and stress level. In order to expand the motion stroke of the flexure hinge and reduce its parasitic motions, a multi-objective optimization model is established. For six types of flexure hinges including circular, elliptical, rectangular, parabolic, hyperbolic and corner-filleted, a Computer-Aided optimal Design and Analysis Platform (CADAP) based on Visual C++ is developed. Taking parabolic flexure hinge as an example, the results of finite element analysis (FEA) verify the correctness of the theoretical analysis and CADAP.

Key words: Flexure hinge, compliant mechanism, computer-aided, optimal design.

1. INTRODUCTION

With the rise of intelligent manufacturing and robotic technology, the flexure-based compliant mechanisms play important roles in microelectromechanical systems [1], medical devices [2, 3] and other fields [4–10]. Compared with traditional rigid joints, flexure hinges can transmit rotational or translational motions and force between two adjacent rigid links through their own elastic deformation [11]. As the key components of compliant mechanisms, flexure hinges have a lot of advantages including compactness, no friction and no assembly requirements [12].

In 1965, Paros and Weisbord [13] first presented right-circular flexure hinges. Since then, various conic flexure hinges have been proposed, such as elliptical [14], corner-filleted [15], parabolic and hyperbolic [16]. In order to achieve a greater range of motion and higher accuracy, scholars have proposed many flexible hinges with complex structures, such as V-shaped [17], cartwheel-type [18], power-function-shaped [19], exponent-sine-shaped [20], polynomial [21] and U-shaped [22]. However, a single design usually lacks an integrated theory. Thus, corresponding design and analysis methods have been presented, including pseudo-rigid body model [12], matrix analytical compliance model [6], a closed-form nonlinear model [23] and topology optimization method [24, 25], etc. Based on

[1] School of Mechanical Engineering, University of Science and Technology Beijing, Beijing 100083, China
[*] Corresponding author, e-mail address: qlf@ustb.edu.cn (L. Qiu).

Ro. J. Techn. Sci. − Appl. Mechanics, Vol. 67, N° 1, P. 7–21, Bucharest, 2022

these, hybrid flexure hinges were explored. Chen et al. [26] proposed right-circular corner-filleted and right-circular elliptical hinges, which are both more rotation-compliant than the right-circular ones. Lin et al. [27] proposed hyperbolic-corner-filleted flexure hinges, which has different performance when the fixed and free ends switch because of the transverse asymmetry. In 2019, Li et al. [28] presented a generalized analytical compliance model that can quickly formulate the equations of compliance and precision for planar hybrid flexure hinges.

In order to better develop the performance of flexure hinges, researches have been conducted in terms of degrees of freedom [29–31], materials [3,32], structures [33–35], and combination patterns. In order to overcome the spring back behavior, Liu et al. [36] proposed a Zero-stiffness Flexure Hinge using the positive and negative stiffness matching method. With the advantage of compliance, flexure hinges can be used in human-machine interaction and improve its safety. In response to the requirement of variable stiffness of the mechanism, Qiu et al. [37] proposed a pitch-varying folded flexure hinge based on the theory and characteristics of the coil spring. Although there have been many researches on flexible hinges, an effective and efficient tool is still needed to solve the complicated design and analysis. Consequently, this paper proposes a computer-aided optimization design and analysis platform based on symmetric conic-section flexure hinges [38].

The paper is organized as follows: Section 2 analyzes the performance of straight-axis flexure hinges, including capacity of rotation, precision and stress level. In Section 3, a multi-objective optimization model of the hinge is established, and the computer-aided optimization design platform is built using the penalty function method and Powell's method. Section 4 introduces the computer-aided optimization design and analysis platform, and gives an example. Section 5 carries on finite element analysis, and the results verify the correctness of the theoretical analysis and platform. Section 6 concludes the work.

2. ANALYSIS OF SYMMETRIC SINGLE-AXIS FLEXURE HINGES

As a key component of compliant mechanisms, flexure hinges directly affect the properties of the mechanism. The performance of flexure hinges mainly includes the capacity of rotation, precision of rotation and stress level. As shown in Fig. 1, the single-axis flexure hinges studied in this paper have axial and transverse symmetry including 6 types, i.e., circular, elliptical, rectangular, parabolic, hyperbolic and corner-filleted.

The dimension parameters of the hinge and external loads are shown in Fig. 2, where $t(x)$ is the variable thickness function, w is the width of the hinge, l is the length of the hinge, and O-xyz is the global reference frame. The left end of the hinge is fixed, and the load is applied to the free end O_1. Suppose the deformation vector $\boldsymbol{X}=[u_x, u_y, u_z, \theta_x, \theta_y, \theta_z]^{\mathrm{T}}$ and the load vector $\boldsymbol{F}=[F_x, F_y, F_z, M_x, M_y, M_z]^{\mathrm{T}}$, where u_x, u_y, and u_z are the displacements of the free end along the x, y, and z axes, respectively, and θ_x, θ_y, and θ_z are the rotation angles of the free end around the x, y, and z axes, respectively.

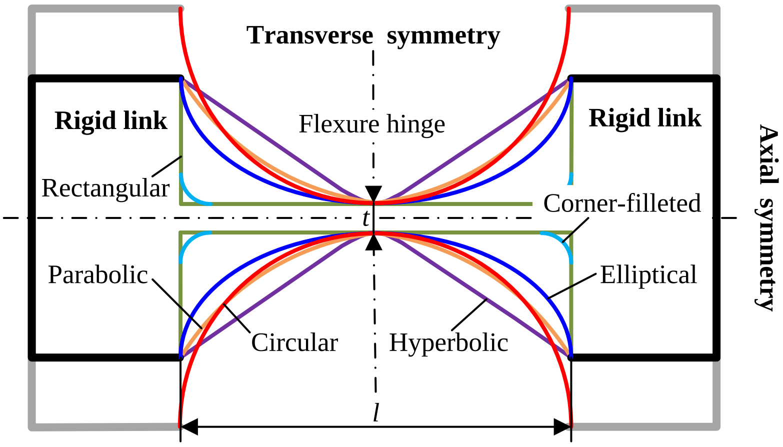

Fig. 1 – Configurations of straight axis flexure hinge.

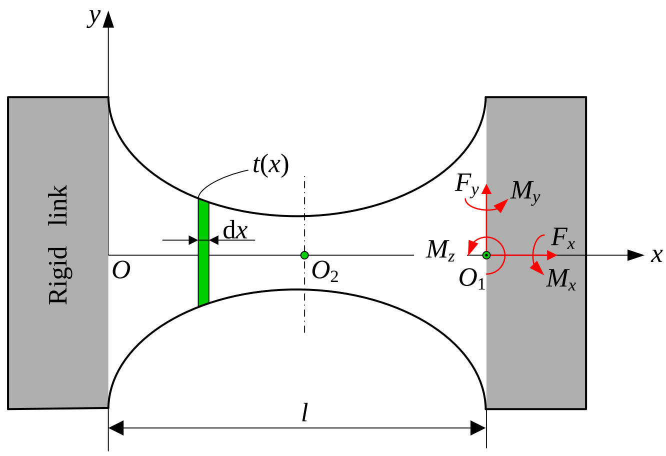

Fig. 2 – The dimension parameters of the hinge and external loads.

2.1. CAPACITY OF ROTATION

The rotation capacity of a single-axis flexure hinge can be represented as the deformation caused by applying a unit load on the free end, which is quantitatively represented by its compliance matrix. According to the load direction, external loads are divided into two categories: (1) the loads F_x, F_y, and M_z acting in the *O-xy* plane, and (2) the loads F_z, M_x, and M_y acting out of the O-xy plane. In this paper, the influence of M_x can be ignored, but the influence of F_z and M_y is not neglected.

According to the energy principle, the strain energy of an elastic body can be formulated as

$$U=\int_l \frac{F_{\mathrm{N}}^2(x)\mathrm{d}x}{2EA}+\int_l \frac{M^2(x)\mathrm{d}x}{2EI}+\int_l \frac{T^2(x)\mathrm{d}x}{2GI} \tag{1}$$

where E and G are the elastic and shear modulus of the material, A is the cross-sectional area, I is the moment of inertia.

If the cross section is rectangular

$$I=\frac{1}{12}wt^3(x) \tag{2}$$

According to the small-deflection assumption and Castigliano's second theorem, the deformation of the free end of the single-axis flexure hinge can be formulated as

$$u_i=\int_l \frac{F_{\mathrm{N}}(x)}{EA}\frac{\partial F_{\mathrm{N}}(x)}{\partial F_i}\mathrm{d}x+\int_l \frac{M(x)}{EI}\frac{\partial M(x)}{\partial F_i}\mathrm{d}x, \tag{3}$$

namely

$$\boldsymbol{X}=\mathbf{C}\boldsymbol{F}, \tag{4}$$

where **C** is the compliance matrix of the single-axis flexure hinge.

According to the motion characteristics of the hinge in and out of the O-xy plane, Eq. (4) can be formulated as

$$\begin{bmatrix}\boldsymbol{X}^{\mathrm{ip}}\\ \boldsymbol{X}^{\mathrm{op}}\end{bmatrix}=\begin{bmatrix}\mathbf{C}^{\mathrm{ip}} & \mathbf{0}\\ \mathbf{0} & \mathbf{C}^{\mathrm{op}}\end{bmatrix}\begin{bmatrix}\boldsymbol{F}^{\mathrm{ip}}\\ \boldsymbol{F}^{\mathrm{op}}\end{bmatrix}, \tag{5}$$

where the superscript "ip" denotes "in plane", and "op" means "out of plane", $\boldsymbol{X}^{\mathrm{ip}}=[u_x, u_y, \theta_z]^{\mathrm{T}}$, $\boldsymbol{X}^{\mathrm{op}}=[u_z, \theta_y]^{\mathrm{T}}$, $\boldsymbol{F}^{\mathrm{ip}}=[F_x, F_y, M_z]^{\mathrm{T}}$, and $\boldsymbol{F}^{\mathrm{op}}=[F_z, M_y]^{\mathrm{T}}$.

The compliance matrices of the single-axis flexure hinge in and out of the O-xy plane are respectively

$$\mathbf{C}^{\mathrm{ip}}=\begin{bmatrix}\mathrm{C}_{x\text{-}F_x} & 0 & 0\\ 0 & \mathrm{C}_{y\text{-}F_y} & \mathrm{C}_{y\text{-}M_z}\\ 0 & \mathrm{C}_{\theta_z\text{-}F_y} & \mathrm{C}_{\theta_z\text{-}\mathrm{M}_z}\end{bmatrix}, \tag{6}$$

$$\mathbf{C}^{\mathrm{op}} = \begin{bmatrix} C_{z\text{-}F_z} & C_{z\text{-}M_y} \\ C_{\theta_y\text{-}F_z} & C_{\theta_y\text{-}M_y} \end{bmatrix}, \tag{7}$$

where the subscript "x-F_x" denotes the displacement along the x-axis caused by F_x, and "θ_z-M_z" denotes the rotation angle around the z-axis caused by M_z, and the rest is in a similar way.

Each non-zero term for the compliance matrix $\mathbf{C}^{\mathrm{ip}}$ can be formulated as

$$C_{x\text{-}F_x} = \frac{1}{Ew}\int_0^l \frac{\mathrm{d}x}{t(x)}, \tag{8}$$

$$C_{y\text{-}F_y} = \frac{12}{Ew}\int_0^l \frac{x^2\mathrm{d}x}{t^3(x)}, \tag{9}$$

$$C_{y\text{-}M_z} = C_{\theta_z\text{-}F_y} = \frac{12}{Ew}\int_0^l \frac{x\mathrm{d}x}{t^3(x)}, \tag{10}$$

$$C_{\theta_z\text{-}M_z} = \frac{12}{Ew}\int_0^l \frac{\mathrm{d}x}{t^3(x)}. \tag{11}$$

Each non-zero term for the compliance matrix $\mathbf{C}^{\mathrm{op}}$ can be formulated as

$$C_{z\text{-}F_z} = \frac{12}{Ew^3}\int_0^l \frac{x^2\mathrm{d}x}{t(x)}, \tag{12}$$

$$C_{z\text{-}M_y} = C_{\theta_y\text{-}F_z} = \frac{12}{Ew^3}\int_0^l \frac{x\mathrm{d}x}{t(x)}, \tag{13}$$

$$C_{\theta_y\text{-}M_y} = \frac{12}{Ew^3}\int_0^l \frac{\mathrm{d}x}{t(x)}. \tag{14}$$

2.2. PRECISION OF ROTATION

In the ideal case, the flexure hinge should rotate around its midpoint, i.e., the center of rotation. However, due to the influence of the external load, the rotation center will have a certain offset actually. The precision of rotation can be represented by the offset of the rotation center. A virtual displacement load is applied to the midpoint O_2, which is transformed into the actual load $\boldsymbol{F}$ at the free end O_1 according to the static balance condition. And the deformation of the midpoint can be formulated as

$$\boldsymbol{X}^{\mathrm{p}} = \mathbf{C}^{\mathrm{p}}\boldsymbol{F} \,, \tag{15}$$

where the superscript "p" denotes "precision", $X^{\mathrm{p}} = \left[u_x^{\mathrm{p}}, u_y^{\mathrm{p}}\right]^{\mathrm{T}}$, u_x^{p} is the displacement of the midpoint along the *x*-axis, u_y^{p} is the displacement of the midpoint along the *y*-axis, and $F = \left[F_x, F_y, M_z\right]^{\mathrm{T}}$.

The precision matrix $\mathbf{C}^{\mathrm{p}}$ of the single-axis flexure hinge can be formulated as

$$\mathbf{C}^{\mathrm{p}} = \begin{bmatrix} \mathrm{C}^{\mathrm{p}}_{x\text{-}F_x} & 0 & 0 \\ 0 & \mathrm{C}^{\mathrm{p}}_{y\text{-}F_y} & \mathrm{C}^{\mathrm{p}}_{y\text{-}M_z} \end{bmatrix}, \tag{16}$$

where

$$\mathrm{C}^{\mathrm{p}}_{x\text{-}F_x} = \frac{1}{Ew}\int_{\frac{l}{2}}^{l} \frac{\mathrm{d}x}{t(x)} \tag{17}$$

$$\mathrm{C}^{\mathrm{p}}_{y\text{-}F_y} = \frac{12}{Ew}\left(\int_{\frac{l}{2}}^{l} \frac{x^2\mathrm{d}x}{t^3(x)} - \frac{l}{2}\int_{\frac{l}{2}}^{l} \frac{x\mathrm{d}x}{t^3(x)}\right), \tag{18}$$

$$\mathrm{C}^{\mathrm{p}}_{y\text{-}F_y} = \frac{12}{Ew}\left(\int_{\frac{l}{2}}^{l} \frac{x\mathrm{d}x}{t^3(x)} - \frac{l}{2}\int_{\frac{l}{2}}^{l} \frac{\mathrm{d}x}{t^3(x)}\right). \tag{19}$$

2.3. STRESS LEVEL

The single-axis flexure hinge undergoes linear elastic deformation under the external load, as shown in Fig. 3. The dangerous point is located at the edge of the smallest cross-section where $x=l/2$, and the maximum axial stress at this point is

$$\sigma_a = c\frac{F_x}{A_{\min}}\,, \tag{20}$$

where the minimum cross-section area $A_{\min}=tw$. Take the circular flexure hinge as an example, the coefficient of stress concentration $c = (2.7t + 5.4r)(8r + t) + 0.325$.

The bending normal stress at the dangerous point is

$$\sigma_b = \frac{M_B}{I_z}, \tag{21}$$

where $M_B = M_z + F_y l$, then

$$\sigma_{b\max} = 6c\frac{M_z + F_y l}{wt^2}. \tag{22}$$

The maximum stress on the flexure hinge is

$$\sigma_{\max} = \sigma_a + \sigma_{b\max} = \frac{c}{wt}\left[F_x + \frac{6\left(M_z + F_y l\right)}{t}\right]. \tag{23}$$

When the maximum stress of the flexure hinge is less than the allowable stress $[\sigma]$ of the material, it indicates that the hinge meets the strength requirement, namely

$$\frac{[\sigma]}{\sigma_{\max}} - 1 \geq 0. \tag{24}$$

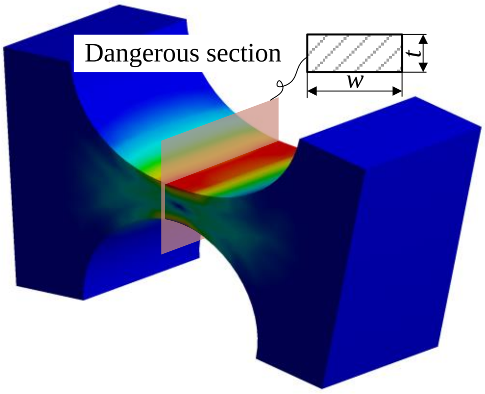

Fig. 3 – Stress simulation of a single-axis circular flexure hinge.

3. OPTIMAL DESIGN OF SINGLE-AXIS FLEXURE HINGES

The single-axis flexure hinge achieves its motions mainly through the elastic deformation of the notch segment. Thus, the dimensions of the hinge have a great influence on its motion stroke and stress level. These dimensions include the length, thickness and width. In order to improve the performance of the flexible hinge, the main dimensional parameters need to be optimized. Single-axis flexure hinges should meet the following basic requirements:

a. Parasitic motions are as small as possible to ensure the precision of rotation;

b. Large motion stroke;

c. Suitable stress level to ensure the safety during the working process.

In this paper, a multi-objective optimization model of the hinge is established by maximizing the compliance in the functional direction and minimizing the compliance in the non-functional direction. Take the circular flexible hinge as an example, its configuration is shown in Fig. 4, where *r*, *t*, and *w* denote the radius, minimum thickness and width of the flexure hinge, respectively, and the length of the hinge $l=2r$. The vector of design variables can be described as $V = [v_1, v_2, v_3]^T = [r, t, w]^T$.

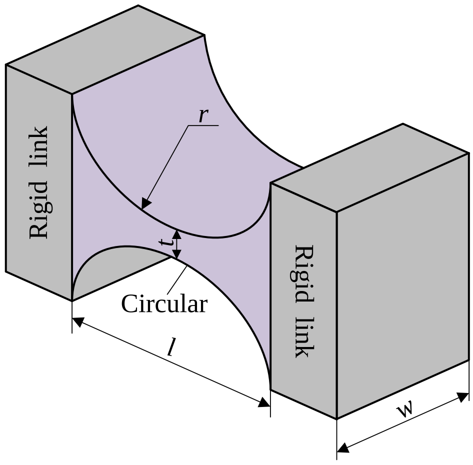

Fig. 4 – Design variables of the circular flexure hinge.

According to the above analysis, the performance of a flexure hinge can be represented by its flexibility matrix. Thus, the goals of optimal design are described as:

a. The capacity of rotation around the *z*-axis is the strongest, i.e., $C_{\theta_z - M_z}$ and $C_{\theta_z - F_y}$ is maximum.

b. The displacement along the *x*-axis is the smallest, i.e., C_{x-F_x} is minimum.

c. The parasitic motions outside the *O*-*xy* plane is the smallest, i.e., C_{z-F_z}, C_{z-M_y}, $C_{\theta_y - F_z}$ and $C_{\theta_y - M_y}$ are minimum.

The integrated objective function can be formulated as

$$\min \ Opt(\boldsymbol{V}) = \frac{C_{x\text{-}F_x} + C_{z\text{-}F_z} + C_{z\text{-}M_y} + C_{\theta_y\text{-}M_y} + C_{\theta_y\text{-}F_z}}{C_{\theta_z\text{-}M_z} + C_{\theta_z\text{-}F_y}} \tag{25}$$

In addition, the flexure hinge is also subject to constraints regarding size and stress limits as below:

$$\text{s.t.} \quad \begin{cases} l_{\min} < l < l_{\max} \\ t_{\min} < t < t_{\max} \\ r_{\min} < r < r_{\max} \\ w_{\min} < w < w_{\max} \\ \sigma_{\max} \le [\sigma] \end{cases} \tag{26}$$

4. COMPUTER-AIDED OPTIMAL DESIGN AND ANALYSIS PLATFORM (CADAP)

Considering the complexity of calculation, a Computer-Aided optimal Design and Analysis Platform (CADAP) based on Visual C++ is developed, which can realize the parametric analysis of compliance, precision and other performance, and check whether the stress level meets the requirements. The compliance matrices of 6 types of flexible hinges are derived, including circular, elliptical, rectangular, parabolic, hyperbolic, and corner-filleted. However, the formulas are too long to be provided in this paper. The CADAP is built using the penalty function method and Powell's method, which includes analysis and optimization modules (Fig. 5).

Step 1: Select the notch shape, initialize the design variables, and set the parameters of the optimization method. Proper settings can not only speed up the calculation speed, but also get better optimization results.

Step 2: Set the boundary conditions, i.e., the upper and lower bounds of dimensions. Fix the left end of the flexure hinge, and apply an external load ***F*** to its free end.

Step 3: Carry out the multi-objective optimization, establish an integrated objective function to expand the motion stroke of the flexure hinge and reduce its parasitic motions.

Step 4: After obtaining the optimized results, calculate and compare the compliance and precision of the initial and the optimized hinge.

Step 5: Check the stress level to ensure the safety of hinge work.

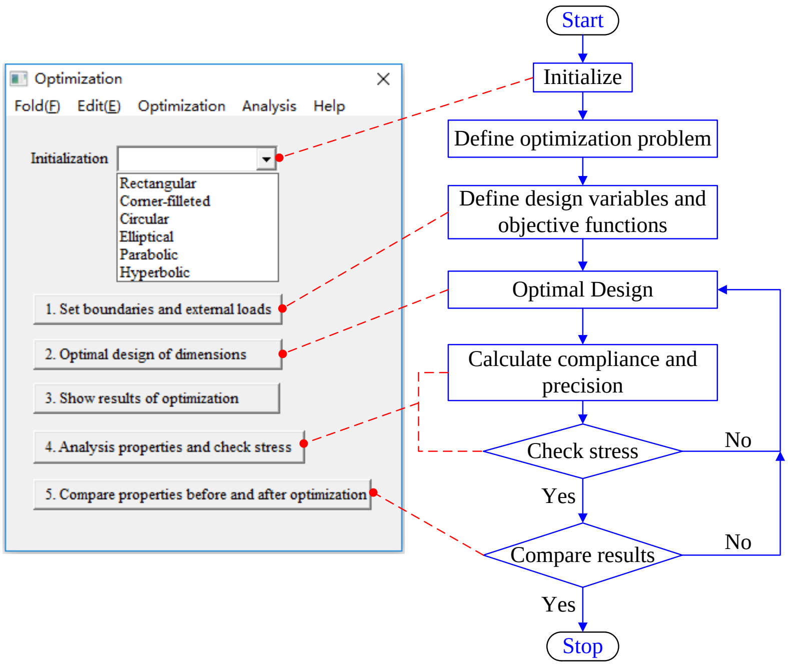

Fig. 5 – Computer-Aided optimal Design and Analysis Platform.

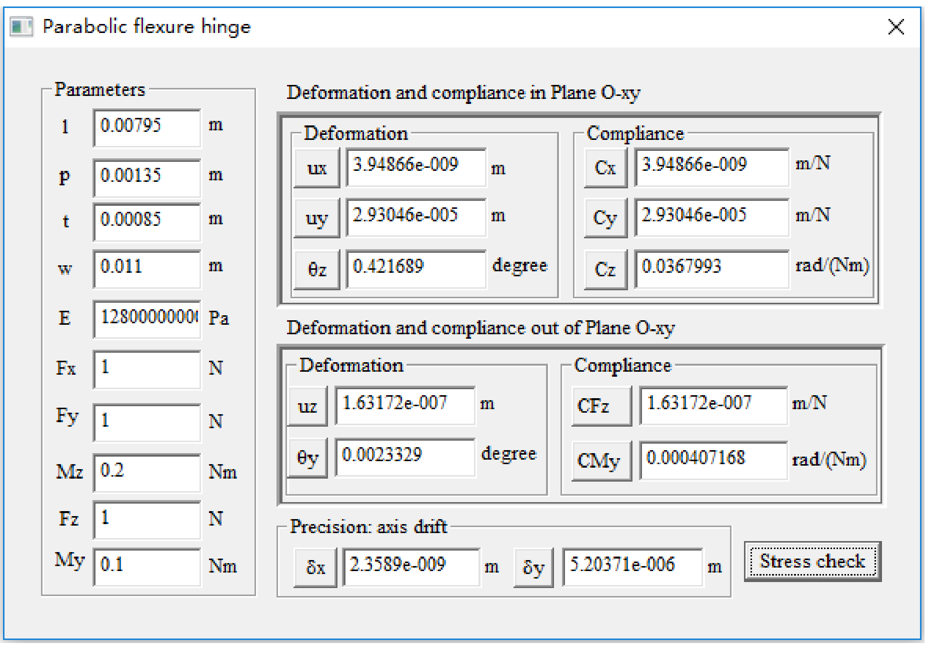

Fig. 6 – Parametric analysis module for compliance and stress.

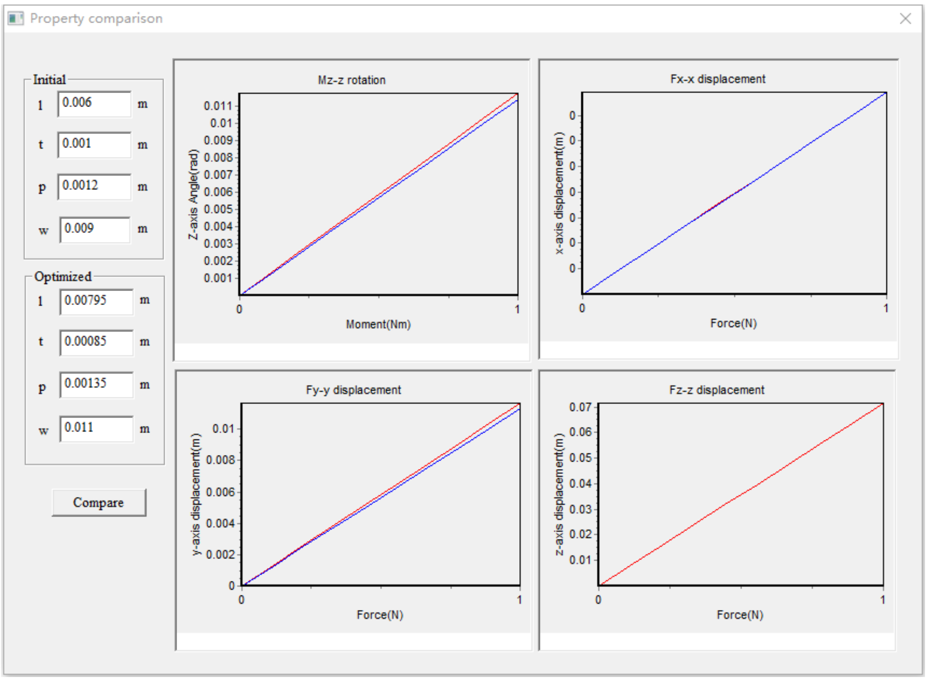

Fig. 7 – Comparison module for optimized performance.

Take the parabolic flexure hinge as an example. Beryllium bronze is selected as the processing material, and the vector of design variables is $\boldsymbol{V}=[l, p, t, w]^T$. The parameters of the optimization method are set as follows: the accuracy of interior point method $EP=10^{-5}$, the accuracy of Powell's method $EPS=10^{-5}$, the reduction coefficient $DE=0.7$, the trial step factor $OH=0.001$, and the weighting factor $R=2.8$. The design variables are initialized as $\boldsymbol{V}^{init}=[l, t, p, w]^T=[0.006, 0.001, 0.0012, 0.009]^T$, the boundary conditions are described in Eq. (27), and the external load $\boldsymbol{F}^{ip}=[F_x, F_y, M_z]^T=[1, 1, 0.2]^T$

$$\begin{cases} 0.005 < l < 0.009 \\ 0.0005 < t < 0.0012 \\ 0.0012 < p < 0.0015 \\ 0.007 < w < 0.015 \end{cases} \tag{27}$$

By optimizing the dimensions, the results are obtained as $V^{opt}=[l,t,p,w]^T=[0.00795,\ 0.00085,\ 0.00135,\ 0.011]m$.

Let $\boldsymbol{F}^{op}=[F_z, M_y]^T=[1, 0.1]^T$; the compliance and precision of the flexure hinge are calculated, as shown in Fig. 6. The initial and optimized performances are compared, as shown in Fig. 7. It can be seen that the performances have been improved to a certain extent after optimization. When checking that the stress level of the hinge meets the strength requirements, it can be seen that the optimal design has been completed.

5. VERIFICATION

In order to verify the correctness of the CADAP proposed in this paper, the FEA is carried out. The three-dimensional model of the hinge is established by Solidworks 2018 and imported it into ANSYS 19.0, as shown in Fig. 8(a). The dimensions are $\boldsymbol{V}=[l, t, p, w]^{T}$ =[0.00795, 0.00085, 0.00135, 0.011]m. Beryllium bronze is selected as the processing material, with elastic modulus E =128GPa and Poisson's ratio μ=0.29. Applying external load $F^{ip}=\left[F_x,F_y,M_z,F_z,M_y\right]^{T}=[1,\ 1,\ 0.2,\ 1,\ 0.1]^{T}$, the results are shown in Fig. 8(b).

The FEA results coincide with the results of theoretical analysis, which indicates the high accuracy of the platform. The comparison between the FEA results and the theoretical analysis is shown in Fig. 9, where u_y and θ_z with relatively large changes are selected. Since the units and values of moment and force load are different, the unlabeled horizontal axis represents the load from 0 to 100%.

6. CONCLUSIONS

In this paper, symmetric single-axis flexure hinges are optimized and analyzed. The compliance matrices of 6 types of flexure hinges are derived, including circular, elliptical, rectangular, parabolic, hyperbolic, and corner-filleted.

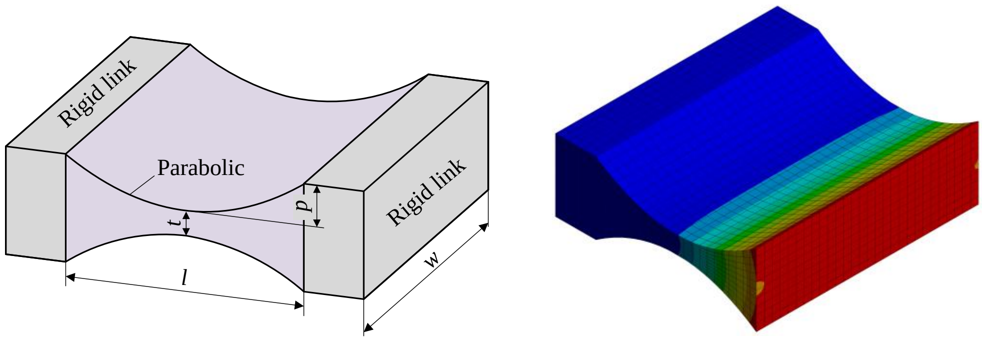

(a) (b)

Fig. 8 – The parabolic flexure hinge (a)3D model (b)finite element model with meshes.

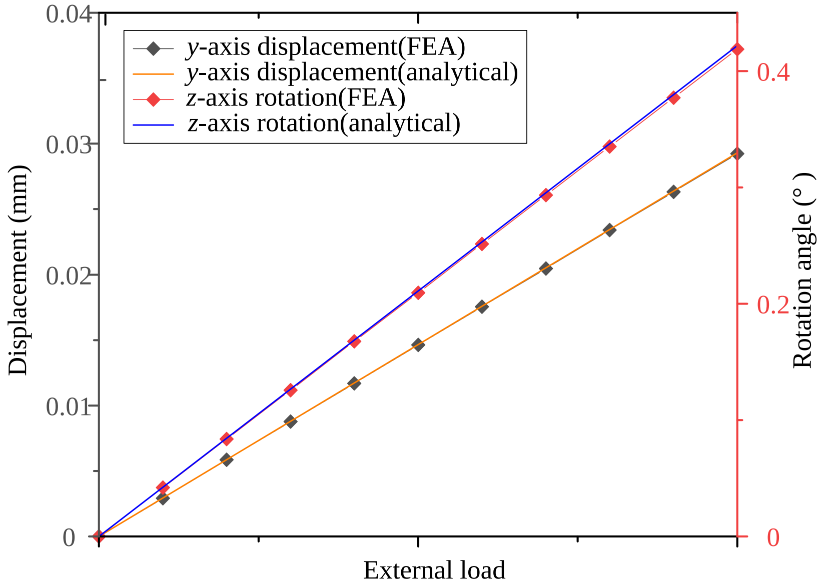

Fig. 9 – Comparison of FEA results and theoretical analysis results.

By calculating the compliance matrix of flexure hinges, the capacity of rotation, the precision of rotation and stress level are analyzed. A multi-objective optimization model of the flexure hinge is established, and the dimensional parameters are optimized to improve the capacity of rotation and reduce the parasitic motions such as axial and lateral displacement. Utilizing the Powell's method and the interior-point penalty function method, a Computer-Aided optimal Design and Analysis Platform (CADAP) is developed based on Visual C++. Taking the parabolic flexure hinge as an example, the optimization results show that when the external load is constant, the performance of the optimized hinge is improved. Finally, the correctness of the theoretical analysis and CADAP is verified through finite element analysis.

Acknowledgements. The authors would like to thank the support provided by the National Natural Science Foundation of China (No. 51475037). This paper is sent to *Romanian Journal of Technical Sciences – Applied Mechanics* on Oct 31st.

REFERENCES

1. VEROTTI, M., CRESCENZI, R., BALUCANI, M., BELFIORE, N.P., *MEMS-based conjugate surfaces flexure hinge*, Journal of Mechanical Design, Transactions of the ASME, **137**, *1*, pp. 1–10, 2015.

2. JONES, J.A., LEE, Y. S., MOORE, J. Z., *Parametric study for asymmetric flexure hinge design for tissue cutting*, Proceedings of the Institution of Mechanical Engineers, Part B: Journal of Engineering Manufacture, **233**, *4*, pp. 1302–1309, 2019.
3. PING, Z., ZHANG, T., ZHANG, C., LIU, J., ZUO, S., *Design of Contact-Aided Compliant Flexure Hinge Mechanism Using Superelastic Nitinol*, Journal of Mechanical Design, **143**, *11*, pp. 1–9, 2021.
4. UTILIZING, M., HINGES, F., YI, B., CHUNG, G.B., NA, H.Y., KIM, W.K., *Design and Experiment of a 3-DOF Parallel*, IEEE Transactions on Robotics, **19**, *4*, pp. 604–612, 2003.
5. LOBONTIU, N., *Compliance-based matrix method for modeling the quasi-static response of planar serial flexure-hinge mechanisms*, Precision Engineering, **38**, *3*, pp. 639–650, 2014.
6. NOVEANU, S., LOBONTIU, N., LAZARO, J., MANDRU, D., *Substructure compliance matrix model of planar branched flexure-hinge mechanisms: Design, testing and characterization of a gripper*, Mechanism and Machine Theory, **91**, pp. 1–20, 2015.
7. MUTLU, R., ALICI, G., PANHUIS, M., SPINKS, G.M., *3D Printed Flexure Hinges for Soft Monolithic Prosthetic Fingers*, Soft Robotics, **3**, *3*, pp. 120–133, 2016.
8. KRIEGER, Y. S., et al., *Fatigue strength of laser sintered flexure hinge structures for soft robotic applications*, IEEE International Conference on Intelligent Robots and Systems, 2017-Septe, pp. 1230–1235, 2017.
9. PULLEYKING, S., SCHULTZ, J., *Flexure Hinge-based Biomimetic Thumb with a Rolling-Surface Metacarpal Joint*, Proceedings - IEEE International Conference on Robotics and Automation, pp. 2960–2966, 2020.
10. CHEN, Z., CHEN, G., ZHANG, X., *Damped leaf flexure hinge*, Review of Scientific Instruments, **86**, *5*, 2015.
11. LOBONTIU, N., *Compliant mechanisms: design of flexure hinges*, CRC press, 2002.
12. HOWELL, L. L., *Compliant Mechanisms*, John Wiley & Sons, 2001.
13. PAROS, J. M., WEISBORD, L., *How to design flexure hinges*, Mach Des, 1965.
14. SMITH, S.T., BADAMI, V.G., DALE, J.S., XU, Y., *Elliptical flexure hinges*, Review of Scientific Instruments, **68**, *3*, pp. 1474–1483, 1997.
15. LOBONTIU, N., PAINE, J.S.N., GARCIA, E., GOLDFARB, M., *Corner-filleted flexure hinges*, Journal of Mechanical Design, Transactions of the ASME, **123**, *3*, pp. 346–352, 2001.
16. LOBONTIU, N., PAINE, J.S.N., O'MALLEY, E., SAMUELSON, M. *Parabolic and hyperbolic flexure hinges: flexibility, motion precision and stress characterization based on compliance closed-form equations*, Precision Engineering, **26**, *2*, pp. 183–192, 2002.
17. TIAN, Y., SHIRINZADEH, B., ZHANG, D., *Closed-form compliance equations of filleted V-shaped flexure hinges for compliant mechanism design*, Precision Engineering, **34**, *3*, pp. 408–418, 2010.
18. KANG, D., GWEON, D., *Analysis and design of a cartwheel-type flexure hinge*, Precision Engineering, **37**, *1*, pp. 33–43, 2013.
19. LI, Q., PAN, C., XU, X., *Closed-form compliance equations for power-function-shaped flexure hinge based on unit-load method*, Precision Engineering, **37**, *1*, pp. 135–145, 2013.
20. WANG, R., ZHOU, X., ZHU, Z., *Development of a novel sort of exponent-sine-shaped flexure hinges*, Review of Scientific Instruments, **84**, *9*, 2013.
21. GRÄSER, P., LINß, S., ZENTNER, L., THESKA, R., *Optimization of compliant mechanisms by use of different polynomial flexure hinge contours*, **71**, Springer International Publishing, 2019.
22. LIANG, J., LI, R., BAI, S., LI, Q., NING, F., KANG, S., *Compliance and fatigue life analysis of u-shape flexure hinge*, Mechanika, **25**, *6*, pp. 501–510, 2019.
23. WANG, D., ZHANG, J., GUO, J., FAN, R., *A closed-form nonlinear model for spatial Timoshenko beam flexure hinge with circular cross-section*, Chinese Journal of Aeronautics, **32**, *11*, pp. 2526–2537, 2019.

24. ZHU, B., ZHANG, X., FATIKOW, S., *Design of single-axis flexure hinges using continuum topology optimization method*, Science China Technological Sciences, **57**, *3*, pp. 560–567, 2014.
25. LIU, M., ZHAN, J., ZHU, B., ZHANG, X., *Topology optimization of flexure hinges with a prescribed compliance matrix based on the adaptive spring model and stress constraint*, Precision Engineering, **72**, June, pp. 397–408, 2021.
26. CHEN, G. M., JIA, J.Y., LI, Z.W., *On hybrid flexure hinges*, 2005 IEEE Networking, Sensing and Control, ICNSC2005 - Proceedings, *2005*, pp. 700–704, 2005.
27. LIN, R., ZHANG, X., LONG, X., FATIKOW, S., *Hybrid flexure hinges*, Review of Scientific Instruments, **84**, *8*, 2013.
28. LI, L., ZHANG, D., GUO, S., QU, H., *Design, modeling, and analysis of hybrid flexure hinges*, Mechanism and Machine Theory, **131**, pp. 300–316, 2019.
29. HSIAO, F.Z., LIN, T.W., *Analysis of a novel flexure hinge with three degrees of freedom*, Review of Scientific Instruments, **72**, *2*, pp. 1565–1573, 2001.
30. LOBONTIU, N., PAINE, J.S.N., *Design of circular cross-section corner-filleted flexure hinges for three-dimensional compliant mechanisms*, Journal of Mechanical Design, Transactions of the ASME, **124**, *3*, pp. 479–484, 2002.
31. LOBONTIU, N., GARCIA, E., *Two-axis flexure hinges with axially-collocated and symmetric notches*, Computers & structures, **81**, *13*, pp. 1329–1341, 2003.
32. YANG, M., DU, Z., DONG, W., *Modeling and analysis of planar symmetric superelastic flexure hinges*, Precision Engineering, **46**, pp. 177–183, 2016.
33. LIU, M., ZHANG, X., FATIKOW, S., *Design and analysis of a multi-notched flexure hinge for compliant mechanisms*, Precision Engineering, **48**, pp. 292–304, 2017.
34. QIU, L., YUE, X., XIE, Z., *Design and analysis of Multicavity Flexure Hinge (MCFH) based on three-dimensional continuum topology optimization*, Mechanism and Machine Theory, **139**, pp. 21–33, 2019.
35. LINß, S., GRÄSER, P., RÄDER, T., HENNING, S., THESKA, R., ZENTNER, L., *Influence of geometric scaling on the elasto-kinematic properties of flexure hinges and compliant mechanisms*, Mechanism and Machine Theory, **125**, pp. 220–239, 2018.
36. LIU, T., BI, S., YAO, Y., DONG, Z., YANG, Q., LIU, L., *Research on zero-stiffness flexure hinge (ZSFH) based on spring four-bar linkage(4BSL)*, Mechanism and Machine Theory, **143**, p. 103633, 2020.
37. QIU, L., LIU, Y., YU, Y., BAI, Y. B., *Design and stiffness analysis of a pitch-varying folded flexure hinge (PFFH)*, Mechanism and Machine Theory, **157**, p. 104187, 2021.
38. LOBONTIU, N., PAINE, J.S.N., GARCIA, E., GOLDFARB, M., *Design of symmetric conic-section flexure hinges based on closed-form compliance equations*, Mechanism and Machine Theory, **37**, *5*, pp. 477–498, 2002.